Preparation of High-performance Activated Carbons from Hemicellulose Pre-extracted Residues of Poplar and their Application in VOCs Removal

Jiakai He,[a] Yuanyuan Zhao,[b] Yun Zhou,[b] and Shubin Wu [a,*]

Hemicellulose was pre-extracted from poplar by the KOH extraction method. A series of activated carbons with high VOCs adsorption capacity were prepared using hemicellulose pre-extraction residue (HPR) as carbon precursor and KOH as the activator. The results showed that the pre-extraction using organic solvent (benzene-ethanol mixture) had no significant effect on the hemicellulose removal efficiency and the microporous structure of activated carbons. After the selective pre-extraction of 38.2 to 65.7 wt% hemicellulose from poplar, the final yield of activated carbons only decreased by 1.1 to 2.0%, but the pore structure of activated carbons was greatly improved. A total of 40.7 wt% hemicellulose in poplar was removed under 4 wt% alkali concentration and 3 h KOH treatment. The activated carbons prepared from HPR of poplar gave the highest BET surface area (3066 $m^2 \cdot g^{-1}$) and pore volume (1.32 $cm^3 \cdot g^{-1}$). The pore structures of activated carbons can be controlled to some extent by changing the removal degree of hemicellulose. The activated carbon obtained under the optimized conditions showed excellent adsorption capacity for toluene (733 $mg \cdot g^{-1}$) and dichloromethane (184 $mg \cdot g^{-1}$). The correlation between adsorption properties and pore structure shows that the adsorption capacities of toluene and dichloromethane were closely related to micropores (< 2 nm) and ultramicropores (< 0.6 nm) of activated carbon, respectively. The pre-extraction of hemicellulose greatly improved the volatile organic compound (VOC) adsorption capacity of activated carbons by increasing the percentage of micropores.

DOI: 10.15376/biores.18.2.2874-2896

Keywords: Poplar; Hemicellulose; Activated carbon; VOCs adsorption

*Contact information: a: State Key Laboratory of Pulp and Paper Engineering, South China University of Technology, Guangzhou 510640, P.R. China; b: Guangzhou Paper Group Ltd., Guangzhou, 511462, P.R. China; *Corresponding author: shubinwu@scut.edu.cn*

INTRODUCTION

Volatile organic compounds (VOCs) refer to organic compounds with a saturated vapor pressure higher than 133.322 Pa at room temperature and boiling points between 50 and 260 °C, mainly including various alkanes, olefins, halogenated hydrocarbons, and aromatic compounds. The VOCs are toxic and highly irritating. They are also important precursors of photochemical smog and cause great harm to the environment and human health (Enesca and Cazan 2020; David and Niculescu 2021). Adsorption is the most widely used VOC treatment technology at present (Zhang *et al*. 2017). The key to adsorption technology is an adsorbent with excellent performance. Activated carbon is widely used in the adsorption and separation of VOCs because of its well-developed pore structure, large specific surface area, and strong specific adsorption capacity. At present, a large number

of studies on the removal of VOCs by activated carbon have been reported (Gil *et al*. 2014; Pui *et al*. 2019; Zhou *et al.* 2019; Li *et al.* 2020; Zhang *et al.* 2020).

Coal is one of the main raw materials for the preparation of activated carbon, but the increasingly serious energy shortage and environmental pollution problems are motivating people to give priority to renewable and sustainable resources as alternatives to fossil energy. Plant fiber biomass has become an important raw material for the preparation of activated carbon because of its high carbon content, low price, and its renewable nature. Production of activated carbon from different plant fiber materials was reported in a range of studies, including wood (Yagmur *et al*. 2013), bamboo (Deng *et al.* 2015), bark (Sessa *et al*. 2022), fruit shell (Magoling and Macalalad 2017), bagasse (Guo *et al.* 2020), straw (Basta *et al*. 2009), pomelo peel (Liu *et al*. 2018), *etc*. Additionally, a lot of research has focused on optimizing the preparation process of activated carbon to improve VOCs adsorption capacity. Yang *et al*. (2021) studied the effect of the chemical activation process on the adsorption capacity of VOCs by properly adjusting the pre-carbonization method and the injection method of KOH. Zhu *et al.* (2018) prepared activated carbon from corncob waste residue and studied the effects of carbonization temperature, impregnation ratio, and carbonization time on the structure and chemical properties of activated carbon. Under the optimized conditions, the specific surface area of the carbon material reached 2022 $m^2 \cdot g^{-1}$, and the toluene adsorption capacity reached 415 $mg \cdot g^{-1}$ (Zhu *et al*. 2018). In Batur's study, activated carbon was produced from defatted black cumin biowaste with $ZnCl_2$ activation through the response surface methodology. When the VOCs inlet concentration was 20 $mg \cdot L^{-1}$, the adsorption capacity of activated carbon with the specific surface area of 1213 $m^2 \cdot g^{-1}$ for benzene, toluene, and xylene was 495 $mg \cdot g^{-1}$, 580 $mg \cdot g^{-1}$, and 674 $mg \cdot g^{-1}$, respectively (Batur and Kutluay 2022). Li *et al.* prepared straw-based activated carbon with a toluene adsorption capacity of 322 $mg \cdot g^{-1}$ and an ethyl acetate adsorption capacity of 240 $mg \cdot g^{-1}$ by optimizing the process (Li *et al*. 2021). In the above studies, only some studies emphasize the importance of the chemical composition of raw materials to the final quality and performance of activated carbon (Wang *et al*. 2018). In addition, some researchers improved the adsorption capacity of specific VOCs by modifying carbonaceous adsorbent. Yang *et al*. synthesized MgO/C composite adsorption material, in which MgO basic sites were more present in the interior of AC than on the surface, thus strengthening the adsorption performance of the adsorption material for polar VOCs (Yang *et al*. 2022a).

When plant fiber biomass is used to prepare carbon materials, the yield is low, although it is an excellent carbon precursor (Wang *et al.* 2022). This phenomenon occurs because cellulose, hemicellulose, and lignin are the main components of plant fiber biomass. The thermal decomposition of the three components forms the carbonaceous structure of carbon materials, but the contributions of the three components to carbon quality and structure are different (Benoît *et al*. 2008). In the process of biomass pyrolysis at high temperatures, cellulose, hemicellulose, and lignin decompose at different rates in different temperature ranges (Collard and Blin 2014). Because of its amorphous structure and low molecular weight, hemicellulose is mostly converted into carbon-containing volatile components, such as carbon monoxide, carbon dioxide, and methane, during the preparation of carbon materials, resulting in its low contribution to carbon quality (Zhang *et al*. 2019b). Therefore, the process of pre-extracting hemicellulose from plant fiber raw materials, and then preparing high-performance activated carbon from the remaining fiber residue, theoretically, is conducive to the realization of high-value utilization of hemicellulose, and will not have a significant impact on subsequent carbon production.

At present, there are many methods to separate hemicellulose from biomass, including acid treatment (Yang *et al.* 2022b), steam explosion (Yan *et al.* 2021), hydrothermal extraction (Sun *et al.* 2022), alkali treatment (Xu *et al.* 2022), *etc*. Although acid treatment can effectively separate hemicellulose, it will lead to a certain degree of hydrolysis and this is not conducive to the utilization of hemicellulose as macromolecules. The cost of the steam explosion is high and hydrothermal extraction requires high temperature and pressure. The alkali method (KOH, NaOH, *etc.*) is the most commonly used chemical method of separating hemicellulose, which can be realized under low temperatures and pressure. Inorganic lye extraction is the most economical and effective method to extract hemicellulose from wood fiber (Yuan *et al*. 2016). Peng *et al.* (2012) treated pea stems with KOH solutions of different concentrations and separated alkali-soluble hemicellulose into linear and branched hemicellulose with the aid of iodine complex precipitation. García *et al.* (2022) used cold alkali extraction to selectively separate hemicellulose from elephant grass and retained 93.0% cellulose and 82.1% lignin in raw materials. It is worth noting that alkali liquor has a strong ability to dissolve xylose, so the alkali method is more suitable for extracting xylan from hardwood. In this study, KOH treatment at room temperature was chosen because of its simple operation, mild conditions, and ability to separate a large amount of xylose. The KOH can be also recovered when hemicellulose in an alkali treatment solution is separated. Wood is an excellent precursor for the preparation of carbon materials. Poplar is one kind of poplar fast-growing wood in China, and it is rich in hemicellulose, so it is used as raw material in this study.

In this study, poplar wood was used as raw material and KOH was used to pre-extract hemicellulose from poplar wood at room temperature. While achieving high conversion and utilization of hemicellulose, hemicellulose pre-extracted residues (HPR) were used as carbon precursors and KOH was used as an activator to prepare activated carbon with high VOCs adsorption capacity, which was used to remove VOCs. Firstly, the influence of organic solvent extracts from poplar on the pre-extraction of hemicellulose and subsequent preparation of activated carbon was evaluated. Then, the influence of hemicellulose removal degree in poplar on activated carbon yield and pore structure was investigated. The difference in hemicellulose removal degree was realized by changing alkali treatment conditions. Finally, toluene and dichloromethane were selected to represent VOCs with different molecular properties. The adsorption performance of activated carbon was evaluated by the dynamic adsorption method and the relationship between the pore structure of activated carbon and the adsorption capacity of VOCs was constructed.

EXPERIMENTAL

Materials

Poplar chips (hardwood) were obtained from Shandong Jianghe Paper Co., Ltd. (China). Potassium hydroxide (KOH), benzene, anhydrous ethanol, and other reagents were purchased from Guangzhou Chemical Reagent Co., Ltd. (China).

Preparation of Carbon Precursors

Poplar-based materials were prepared as carbon precursors through different pretreatment:

(a) The poplar powder after air drying, crushing, screening, and drying was marked as P and 40 to 60 mesh standard sieve was used for screening.

(b) Poplar powder (P) was extracted with the benzene-ethanol mixture (2:1, v: v) for 6 h, dried at 105 ℃ for 24 h after air drying, and the raw material after extraction was marked as P_E. The process of pre-extraction of organic solvents is described in detail in the Chinese national standard GB/T 35818 (2018).

(c) 20 wt% KOH solution was added to P and P_E at a solid-liquid ratio of 1:10. The solid-liquid ratio refers to the ratio of the mass (g) of poplar powder to the volume (mL) of KOH solution. After the mixture was treated at 30 ℃ for 3 h, the filtrate (hemicellulose solution) and HPR was obtained by solid-liquid separation. The HPR was washed to neutral with water and dried at 105 ℃ for 24 h and marked $PK_{20\text{-}3}$ and $P_EK_{20\text{-}3}$.

(d) Amounts of 4, 7, 10, or 20 wt% KOH solution was added to P at a solid-liquid ratio of 1:10. After the mixture was treated at 30 ℃ for 3 h, the filtrate (hemicellulose solution) and HPR was obtained by solid-liquid separation. The HPR was washed to neutral with water and dried at 105 ℃ for 24 h, marked $PK_{x\text{-}y}$. Here x represents the concentration of KOH solution and y represents the time of alkali treatment.

Composition Analysis of Carbon Precursors

The holocellulose and Klason-lignin contents were determined according to the procedure detailed in the Chinese national standard GB/T 35818 (2018). α-Cellulose was obtained by treating delignified raw materials with 17.5% sodium hydroxide solution (GB/T 744 (2004)). The hemicellulose content was represented by the difference between holocellulose content and α-cellulose content. It should be noted that the hemicellulose content obtained is an approximate value. Residues refer to other components in raw materials except for cellulose, hemicellulose, and lignin, including extracts and ash. The content of the organic solvent extract was determined by extraction with organic solvent (benzene-ethanol mixture), and the ash content was determined by the remaining sample mass after the raw material was burned in a muffle furnace at 575 ℃ (GB/T 35818 (2018)).

Preparation of Activated Carbons

The carbon precursors (on a dry basis) were placed in a porcelain crucible in a tubular furnace, heated to 500 ℃ in argon gas flow at a heating rate of 10 ℃/min, and then carbonized at 500 ℃ for 1 h. The carbonized solids were obtained after cooling to room temperature. Carbonated solids were impregnated with KOH solution using a weight ratio of carbonated solid/KOH of 1/4 (on a dry basis), and then dried for 24 h in an oven at 105 ℃. The mixture of carbonized solids and KOH was put into a porcelain crucible, then heated to 800 ℃ at a heating rate of 10 ℃/min in an argon atmosphere and activated at 800 ℃ for 1 h. The resultant activated carbons were thoroughly washed with 1 M HCl followed by ultrapure water until the pH was neutral. Finally, the activated carbons were dried at 105 ℃ for 24 h and stored in sealed vials. Activated carbons were labeled as (carbon precursor-AC).

Characterization of Activated Carbons

The N_2 adsorption/desorption isotherms of activated carbons were measured at 77 K using an ASAP 2460 analyzer, and the pore structure parameters were calculated according to the N_2 adsorption/desorption isotherms. The samples were previously outgassed at 300 ℃ for 10 h. The specific surface area of activated carbons was calculated by the BET method, the specific surface area and volume of micropores were obtained by

the t-plot method, and the pore size distribution (PSD) was obtained by the BJH method. The micromorphology of the samples was analyzed by scanning electron microscope (SEM, FEI Inspect F50, FEI Company, Hillsboro, OR, USA).

Adsorption Test

The adsorption capacity of poplar-based activated carbon for toluene and dichloromethane was evaluated using the experimental device shown in Fig. 1. Before adsorption, the samples were degassed in a vacuum box at 105 ℃ for 12 h to remove the adsorbed moisture and impurities. The air in the test system was discharged with high-purity nitrogen. The VOCs dynamic adsorption experiment conditions were set as follows: the amount of active carbon was 100 mg (± 1%), the active carbon was fixed in a quartz tube with an inner diameter of 6 mm, the adsorption temperature was controlled at 30 ℃ through the glass fiber heating belt, the concentration of toluene and dichloromethane was 500 ppm (± 2%), and the gas flow rate at the inlet side was controlled at 100 mL/min. The outlet concentration of the gas was detected by a gas chromatograph (GC2002, Kechuang, Shanghai, China).

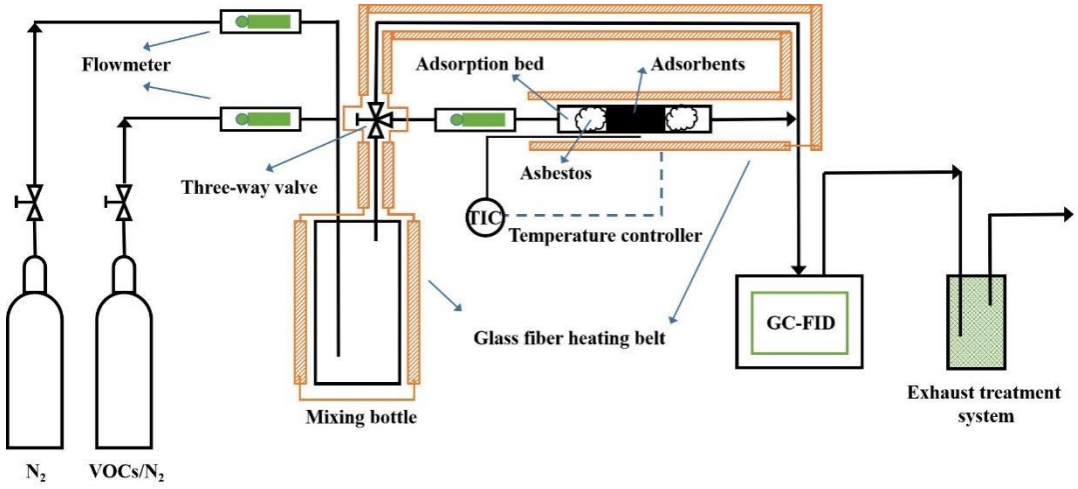

Fig. 1. Schematic of VOCs dynamic adsorption experimental setup

The breakthrough time (t_b) is defined as the time when the VOCs outlet to inlet concentration ratio (C/C_0) is 5%, and the saturation time (t_s) is defined as the time when the VOCs outlet to inlet concentration ratio (C/C_0) is 95%. The adsorption capacity at t_b and t_s is expressed as breakthrough adsorption capacity (Q_b) and saturated adsorption capacity (Q_s). The adsorption capacity (Q) of activated carbon can be calculated according to the following formula,

$$Q = \frac{C_0 V 10^{-6}}{\mathrm{m}} \left(t - \int_0^t C_t / C_0 dt \right) \quad (1)$$

where Q is the adsorption capacity (mg·g^{-1}), V is the VOCs gas flow rate (mL·min^{-1}), C_0 is the VOCs gas inlet concentration (g·m^{-3}), t is the adsorption time (min), C_t is the VOCs gas outlet concentration (g·m^{-3}) at t (min), and m is the sample mass (g).

The Yoon-Nelson (Y-N) model was used for the nonlinear fitting of the adsorption breakthrough curve. The adsorption rate and 50% adsorbate breakthrough time can be

obtained through linear regression analysis. The formula of the Y-N model is as follows (Yoon and Nelson 1984),

$$\ln \frac{C_t}{C_0 - C_t} = K_{YN} t - \tau K_{YN} \quad (2)$$

where K_{YN} is the physical diffusion rate of adsorption process (min^{-1}), τ is the penetration time of 50% adsorbate (min), C_0 is the inlet concentration of VOCs ($g \cdot m^{-3}$), C_t is the outlet concentration ($g \cdot m^{-3}$) of VOCs at t (min), and t is the adsorption time (min).

RESULTS AND DISCUSSION

Effect of Organic Solvent Extraction on Alkali Extraction and Preparation of Activated Carbons

Before using plant fiber for research, many researchers considered using organic solvent for extraction to eliminate the influence of organic solvent extract. Table 1 shows the contents of holocellulose, α-cellulose, hemicellulose, and Klason-lignin of four carbon precursors (P, $PK_{20\text{-}3}$, P_E, and $P_EK_{20\text{-}3}$). It should be pointed out here that the ash content of the poplar used in this study was below 1%. Table 1 shows that the content of holocellulose and hemicellulose in P was 74.5% and 34.0%, and the content of Klason-lignin was 21.7%, which is consistent with previous reports (Yagmur *et al*. 2013). The composition of PE was close to P, indicating that the composition of poplar had not been noticeably changed by organic solvent extraction. This may be because of the low content (less than 1%) of organic solvent extract in the poplar used, and the fact that the extract mainly was present in the parenchyma cells, and the main components were free and esterified fatty acids.

Figure 2 shows the material balance of two poplar raw materials (P, P_E) in the process of alkali treatment at room temperature, reflecting the change in content and removal rate of α-cellulose, hemicellulose, and Klason-lignin in P and PE after alkali treatment (alkali extraction conditions are shown in Fig. 2). It can be seen from Fig. 2 that after 100 g of P was extracted with alkali at room temperature, 76.51 g of HPR ($PK_{20\text{-}3}$) could be obtained, and similarly, 76.86 g of $P_EK_{20\text{-}3}$ could be obtained from 100 g of P_E. Whether the raw materials could be pre-extracted with an organic solvent or not, the hemicellulose removal rate reached up to 65% and the lignin retention rate reached 91% after extracting for 3 h with 20 wt% KOH at 30 ℃. The results show that alkali pre-extraction can remove a large amount of hemicellulose and only a small amount of lignin, which can be attributed to the strong ability of alkali liquor to dissolve xylose (main components of hemicellulose in poplar). At the same time, the removal rate of hemicellulose by alkali extraction was not noticeably improved by organic solvent extraction.

Table 1. Composition Analysis of Carbon Precursors

Carbon Precursor	Holocellulose (wt%)	α-Cellulose (wt%)	Hemicellulose (wt%)	Klason-lignin (wt%)
P	74.5	40.4	34.0	21.7
$PK_{20\text{-}3}$	66.7	51.5	15.3	26.0
P_E	75.1	40.8	34.3	21.9
$P_EK_{20\text{-}3}$	67.8	53.0	14.7	26.2

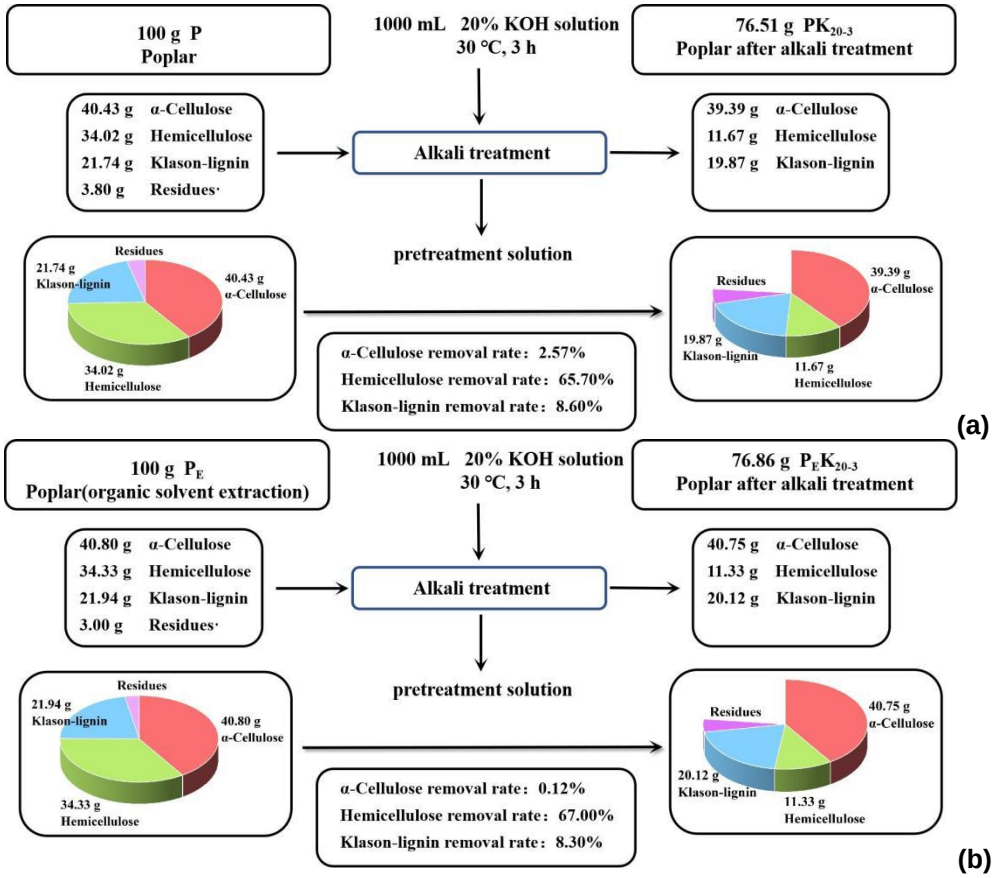

Fig. 2. Material balance of poplar in the alkali extraction process (a) Sample was not extracted; (b) Extracted sample

Activated carbons were prepared from the above four carbon precursors under the same conditions. Table 2 shows that the yield of activated carbons was not noticeably changed whether it was extracted with an organic solvent or not. Figure 3a shows the N_2 adsorption/desorption isotherms of poplar-based activated carbons at 77 K. The N_2 adsorption/desorption isotherms of poplar-based activated carbons can be classified as type I. The adsorption capacity of N_2 increased remarkably at lower relative pressure ($P/P0 < 0.05$). All isotherms show narrow elbows and horizontal platforms, and almost no hysteresis loops, which indicates that the pores of activated carbons were mainly microporous. Figure 3b shows that the pore sizes of poplar-based activated carbons were mainly distributed in the range of less than 2 nm, and the pore structures of the activated carbons prepared after pretreatment were better than that of the activated carbon prepared without pretreatment (PAC). Surprisingly, the pore volume of PAC was found to be higher than that of other activated carbons when the pore size was less than 0.6 nm, while the pore volume of other activated carbons was higher than that of PAC when the pore size was greater than 0.6 nm. This may indicate that PAC is more advantageous for ultramicropores (< 0.6 nm).

The main pore structure parameters of poplar-based activated carbons calculated in Fig. 3a are listed in Table 2 to further understand the pore structures of activated carbons. Table 2 shows that the specific surface area and pore volume of P_EAC were remarkably increased compared with PAC. The S_{BET} value increased from 1401 to 2584 $m^2 \cdot g^{-1}$ (approximately 84.4% increase), and V_{total} increased from 0.59 to 1.13 $cm^3 \cdot g^{-1}$

(approximately 91.5% increase), indicating that the pre-extraction of organic solvent optimized the pore structures of activated carbons prepared from poplar (no pretreatment). However, the pore structure of $P_EK_{20\text{-}3}AC$ was not better than that of $PK_{20\text{-}3}AC$, indicating that the pre-extraction of organic solvent did not promote the preparation of activated carbons from poplar wood after alkali extraction. It has been shown before that the composition of poplar and the removal rate of hemicellulose will not be noticeably changed by the pre-extraction of organic solvent, so it is speculated that part of the extracts in the parenchyma cells is removed by organic solvent, many small channels are formed on the cell wall, and fibers are moistened, which leads to changes in the pore structures of activated carbons. However, a large amount of hemicellulose in poplar is removed by alkali extraction, which will also lead to fiber swelling and composition change. When poplar fiber is treated with alkali, its morphology and composition change more obviously. Therefore, the effect of organic solvents on the pore structure of activated carbon is masked to a certain extent under the strong action of an alkaline solution.

The micromorphology of activated carbons was characterized by SEM. It can be seen from Fig. 4a through 4h that activated carbons still maintained the structure of plant fibers, the pore structure of poplar fibers provided a reaction site for the activation of KOH, and the external surface of raw materials became rough under the erosion of activators, which shows the role of activators in erosion and pore formation. The organic solvent forms fine channels on the plant fiber, and these channels provide more activation sites for the activator, resulting in more pore structures of the activated carbons. Similarly, the process of hemicellulose removal will leave more pores, which are developed based on the original pores and may explain the covering effect of alkali liquor on organic solvents.

In summary, for poplar, the removal rate of hemicellulose and the yields of activated carbons under alkali extraction were less affected by the pre-extraction of organic solvent. Although organic solvent can optimize the pore structure of activated carbons prepared from untreated raw materials, it led to no noticeable improvement in the preparation of activated carbon from HPR. Therefore, the pre-extraction of organic solvent can be ignored when preparing activated carbon from HPR after alkali extraction.

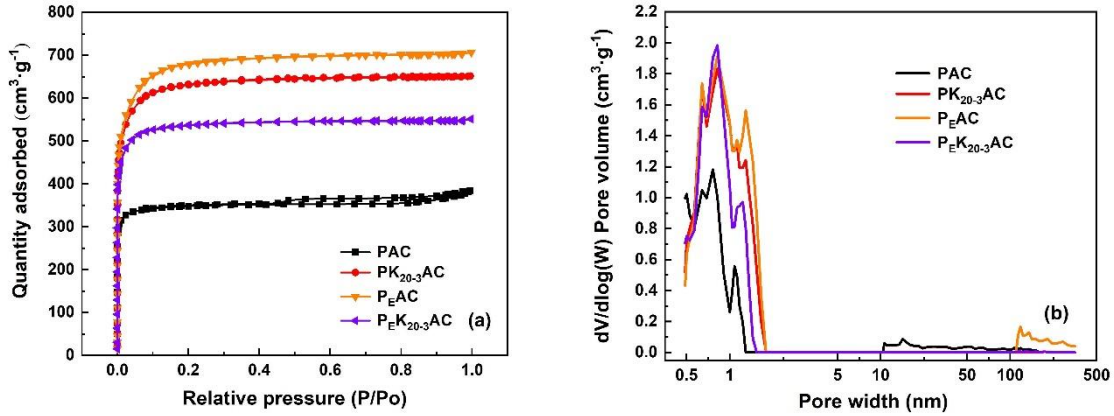

Fig. 3. N_2 adsorption/desorption isotherms (a) and pore size distributions (b) of activated carbons prepared with P, $PK_{20\text{-}3}$, P_E, and $P_EK_{20\text{-}3}$ as carbon precursors

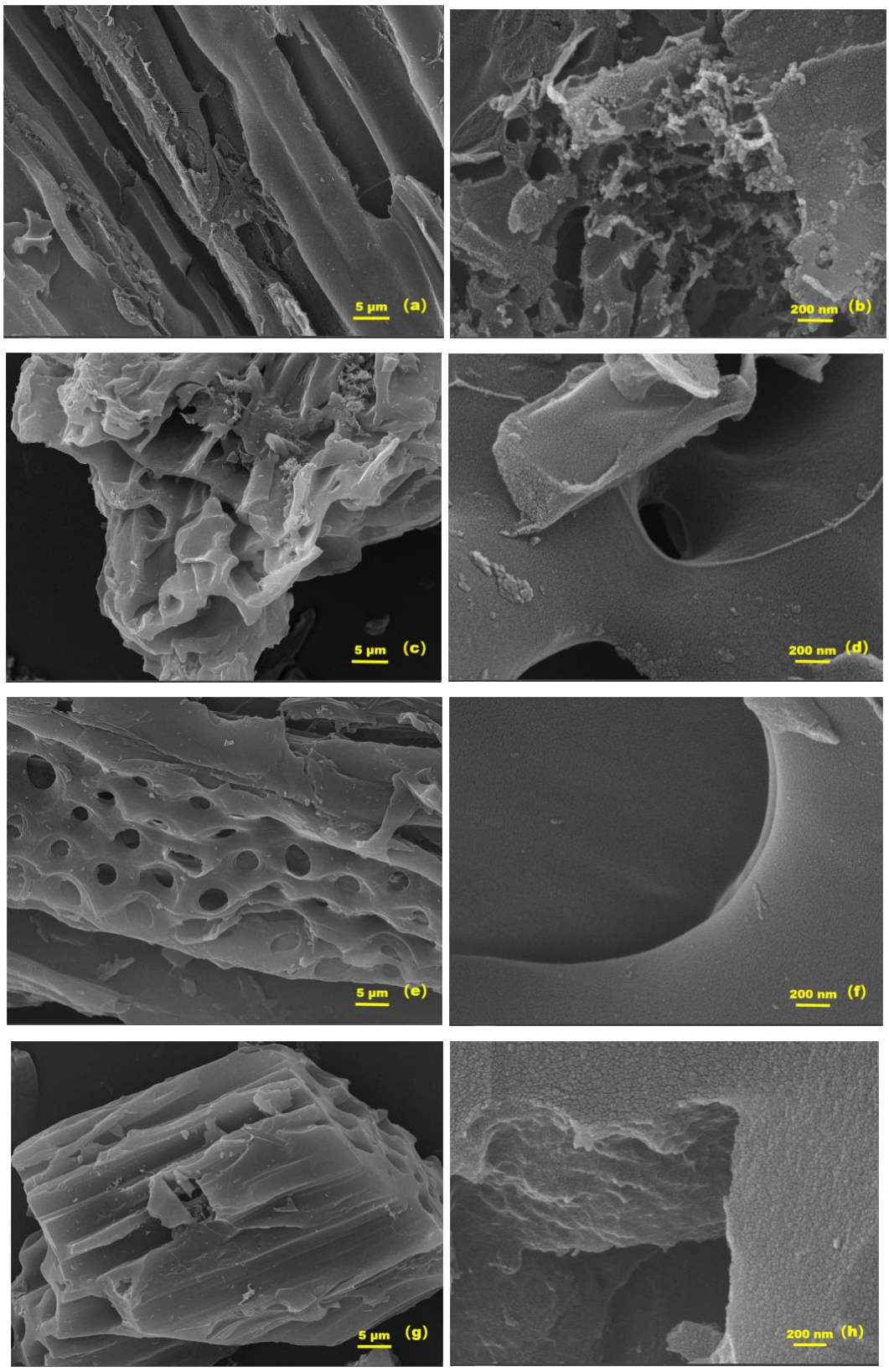

Fig. 4. SEM images of PAC (a, b), $PK_{20\text{-}3}AC$ (c, d), P_EAC (e, f), and $P_EK_{20\text{-}3}AC$ (g, h)

Table 2. Yield and Main Pore Structure Parameters of Activated Carbons Prepared with P, $PK_{20\text{-}3}$, P_E, and $P_EK_{20\text{-}3}$ as Carbon Precursors

Sample	[1]Carbon Yield (%)	[2]S_{BET} ($m^2 \cdot g^{-1}$)	[3]S_{micro} ($m^2 \cdot g^{-1}$)	[4]S_{meso} ($m^2 \cdot g^{-1}$)	[5]S_{ultra} ($m^2 \cdot g^{-1}$)	[6]V_{total} ($cm^3 \cdot g^{-1}$)	[3]V_{micro} ($cm^3 \cdot g^{-1}$)	[4]V_{meso} ($cm^3 \cdot g^{-1}$)	[5]V_{ultra} ($cm^3 \cdot g^{-1}$)	[7]D_p (nm)
PAC	18.0	1401	1337	61	582	0.59	0.51	0.08	0.22	1.67
P_EAC	18.1	2584	2406	145	351	1.13	0.97	0.09	0.11	1.66
$PK_{20\text{-}3}$AC	16.5	2458	2298	129	390	1.01	0.91	0.08	0.12	1.64
$P_EK_{20\text{-}3}$AC	16.1	2112	1923	89	381	1.03	0.85	0.14	0.15	1.61

Note: [1]Carbon yield: (m_{ac}/m_p) × 100%, m_{ac} is the mass of activated carbon, m_p is the mass of poplar; [2]S_{BET}: specific surface area calculated by the BET method; [3]S_{micro} and [3]V_{micro}: surface area and pore volume of micropores calculated by the DFT model; [4]S_{meso} and [4]V_{meso}: surface area and pore volume of mesoporous calculated by the BJH model; [5]S_{ultra} and [5]V_{ultra}: specific surface area and pore volume of pores with pore diameter less than 0.6 nm calculated by the DFT model; [6]V_{total}: total pore volume calculated at $P/P_0 = 0.95$; [7]D_p: average pore diameter

Effect of Hemicellulose Pre-extraction on Preparation of Activated Carbons

Effect of alkali treatment degree on the dissolution rate of components, the removal rate of Klason-lignin and hemicellulose

The degree of hemicellulose removal was regulated by changing alkali concentration and alkali treatment time. Alkali pretreatment resulted in a quality loss of raw materials, mainly a large amount of hemicellulose and a small amount of lignin. Table 3 shows the dissolution rate, Klason-lignin removal rate, and hemicellulose removal rate under different alkali treatment conditions.

Table 3. Dissolution Rate, Klason-lignin Removal Rate, and Hemicellulose Removal Rate Under Different Alkali Treatment Conditions

[1]Carbon Precursor	[2]Dissolution Rate (wt%)	[3]Hemicellulose removal Rate (wt%)	[4]Klason-lignin Removal Rate (wt%)
$PK_{4\text{-}1}$	14.34	38.18	6.21
$PK_{7\text{-}1}$	18.11	49.09	6.49
$PK_{10\text{-}1}$	20.11	55.00	6.44
$PK_{20\text{-}1}$	21.91	59.91	7.04
$PK_{4\text{-}3}$	15.46	40.74	7.41
$PK_{7\text{-}3}$	20.41	54.84	8.05
$PK_{10\text{-}3}$	21.03	57.00	7.54
$PK_{20\text{-}3}$	23.49	65.70	8.60

Note: [1]$PK_{x\text{-}y}$: x is alkali concentration, y is alkali treatment time. [2]Dissolution rate= $\frac{m_0 - m}{m_0} \times 100\%$, m_0 is the mass of raw materials, m is the mass of residues after alkali extraction. [3]Hemicellulose removal rate= $\frac{m_{h0} - m_h}{m_{h0}} \times 100\%$, m_{h0} is the mass of hemicellulose in the raw materials, m_h is the mass of hemicellulose in the residues after alkali extraction. [4]Klason-lignin removal rate= $\frac{m_{k0} - m_k}{m_{k0}} \times 100\%$, m_{k0} is the mass of Klason-lignin in the raw materials, m_k is the mass of Klason-lignin in the residues after alkali extraction.

Under the set conditions (alkali treatment time was 1 to 3 h, alkali concentration was 4 to 20 wt%), 14.34 to 23.49 wt% of the components were removed from the poplar, including 38.18 to 65.70 wt% of hemicellulose and 6.21 to 8.60 wt% of Klason-lignin. With increased alkali concentration and alkali treatment time, the component dissolution rate and hemicellulose removal rate showed an upward trend, and the growth rate gradually tended to be stable. A large amount of hemicellulose can be removed under 1 h, and more alkali treatment time cannot noticeably improve the dissolution rate (an average increase of 1.48% from 1 h to 3 h) and hemicellulose removal rate (an average increase of 4.03% from 1 h to 3 h). Similarly, the dissolution rate and hemicellulose removal rate are not noticeably improved under high alkali concentrations. For Klason-lignin, the removal rate did not change noticeably with the change of conditions. In conclusion, it is feasible to regulate the removal degree of hemicellulose by changing alkali concentration and alkali treatment time.

Effect of hemicellulose removal degree on the yield and pore structure of activated carbons

In this study, HPR with a hemicellulose removal rate of 38.18 to 65.70 wt% was prepared as carbon precursors to explore the influence of hemicellulose removal on the subsequent preparation of activated carbons. Table 4 shows the yield of poplar-based activated carbons prepared under different removal degrees of hemicellulose. The results show that the yield of PAC is 18.0%, and the yield of $PK_{x\text{-}y}AC$ is 16.0 to 16.9%. Figure 5a and b show the relationship between dissolution rate/hemicellulose removal rate and activated carbon yield. Carbon yield is evaluated in two ways: by evaluating the yield of the carbon production process through comparing the quality of activated carbons with that of carbon precursors (HPR). The other way is to evaluate the yield of the whole process (pretreatment and carbon production) by comparing the quality of activated carbons with that of the original poplar. The results show that with increased dissolution rate, the yield (relative to carbon precursor) slightly increased, and the yield increased 1.4% for every 10% dissolution rate. The yield (relative to poplar) slightly decreased, and the yield decreased 0.6% for every 10% dissolution rate. Furthermore, the change of yield with hemicellulose removal rate is consistent with the dissolution rate because xylan is the main component of dissolution. When 38.18 to 65.70 wt% hemicellulose was selectively extracted from poplar, the yield of final activated carbons only decreased 1.1 to 2.0%, proving that hemicellulose was mainly separated as volatile during the preparation of activated carbons, and its contribution to the final carbon quality was inferior to that of other components. Benoît *et al.* (2008) also proved this in their research. They carbonized/activated hemicellulose, cellulose, and lignin respectively, then calculated the weight contribution of each component to the quality of chars and activated carbons according to the composition of raw materials. In their results, the weight contribution of hemicellulose to chars was 14.1% to 24.5%, and that of lignin was 55.0% to 79.0%; the weight contribution of hemicellulose to activated carbons was 13.6% to 23.6%, and that of lignin was 53.5% to 78.8% (Benoît *et al*. 2008). It is obvious that hemicellulose is not the main weight contributor of carbon.

After a large amount of hemicellulose was removed, the lignin content in the HPR increased, so the carbon yield of the residues increased to a certain extent (from 18.0% of PAC to 19.2 to 21.6% of $PK_{x\text{-}y}AC$). However, although the weight contribution of hemicellulose is lower than that of lignin, hemicellulose can also form part of activated carbon in the preparation process. Therefore, after a large amount of hemicellulose in poplar is extracted, the carbon yield of poplar inevitably decreases. Fortunately, the yield

of activated carbons is not noticeably reduced compared with the amount of hemicellulose removed. When poplar is used to prepare activated carbons, a large amount of hemicellulose is converted into highly mixed non-condensable gases, such as CO, CO_2, and CH_4, which are difficult to capture and effectively use. If this unstable hemicellulose is separated, it can be used for many purposes after simple purification (Chen and Lee 2020; Zhao *et al*. 2020). At present, there is a large number of studies on the extraction and purification of hemicellulose from plant fibers (Scapini *et al*. 2021; Arzami *et al*. 2022). From a cost perspective, after hemicellulose is separated, the total amount of activated carbon prepared from raw materials that suffer weight loss does not decrease to a large extent, which has more economic value.

The pore structure of activated carbons has an important influence on the adsorption performance. Figure 6a and b show the N_2 adsorption/desorption isotherms of activated carbons prepared under different hemicellulose removal degrees at 77 K. These isotherms can be classified as Type I, which are the characteristics of microporous materials. It can be found that the N_2 adsorption capacity of $PK_{x\text{-}y}AC$ is always higher than that of PAC. Figure 6c and 6d show that the pore size of activated carbons is mainly distributed in the range of less than 2 nm. The main pore structure parameters of poplar-based activated carbons calculated in Fig. 6a and b are listed in Table 4. Table 4 shows that the specific surface area and pore volume of $PK_{x\text{-}y}AC$ are noticeably increased compared with PAC. S_{BET} increased from 1401 $m^2 \cdot g^{-1}$ to 2154 to 3066 $m^2 \cdot g^{-1}$ (about 53.7 to 118.8% increase), and Vtotal increased from 0.59 $cm^3 \cdot g^{-1}$ to 0.87 to 1.32 $cm^3 \cdot g^{-1}$ (approximately 47.5 to 123.7% increase). A total of 40.74 wt% hemicellulose in poplar was removed under 4 wt% KOH concentration and 3 h alkali treatment, the activated carbon prepared from HPR gave the highest BET surface area and pore volume, 3066 $m^2 \cdot g^{-1}$ and 1.32 $cm^3 \cdot g^{-1}$, respectively. It can be said that HPR after partial hemicellulose removal are more potential carbon precursors. Yagmur also proved this in his research, where under the self-hydrolysis at 130 to 170 ℃, the specific surface area and pore volume of the final carbon materials was increased by reducing the hemicellulose content of the hardwood materials. Additionally, the activated carbon obtained by self-hydrolysis at 150 ℃ had the highest specific surface area and pore volume, which were 2143 $m^2 \cdot g^{-1}$ and 1.474 $cc \cdot g^{-1}$, respectively (Yagmur *et al*. 2013).

The pores of $PK_{x\text{-}y}AC$ prepared in this study were mainly microporous, but the mesoporous surface area, mesoporous volume, and average pore size of $PK_{4\text{-}1}AC$ and $PK_{4\text{-}3}AC$ were higher than those of other activated carbons. Because 14.34 to 15.46% of the components are dissolved under 4 wt% alkali concentration, and 18.11 to 23.49% of the components are dissolved under 7 to 20wt% alkali concentration, it is speculated that this slight change is caused by the difference in hemicellulose removal. The dissolution of a small number of components is conducive to the formation of mesopores, but with the increase of component dissolution rate, mesopores tend to decrease, and activated carbon is transformed into carbon materials with a higher micropore ratio. It can be said that the pore structures of activated carbons can be changed to a certain extent by changing the removal degree of hemicellulose, which is reflected in the small change of micropores and mesopores. Figure 6c and 6d also show this, the pore size distribution of the activated carbons prepared after 4 wt% KOH treatment is wider, with higher specific surface area, mesoporous surface area, and average pore size, while the pore size distribution of the activated carbons prepared after 7 wt% and 10 wt% KOH treatment is more concentrated, with the highest point concentrated at 0.8 to 1 nm, and the pores are more concentrated under the longer KOH treatment time.

In summary, after the selective pre-extraction of 38.18 to 65.70 wt% hemicellulose from poplar, the final yield of activated carbon only decreased 1.1 to 2.0%, but the pore structure of activated carbon was optimized. The activated carbons prepared from HPR have a high proportion of micropores, and $PK_{4\text{-}3}AC$ has the highest specific surface area and pore volume (3066 $m^2 \cdot g^{-1}$ and 1.32 $cm^3 \cdot g^{-1}$). Additionally, the pore structures of activated carbons can be controlled to some extent by changing the removal degree of hemicellulose.

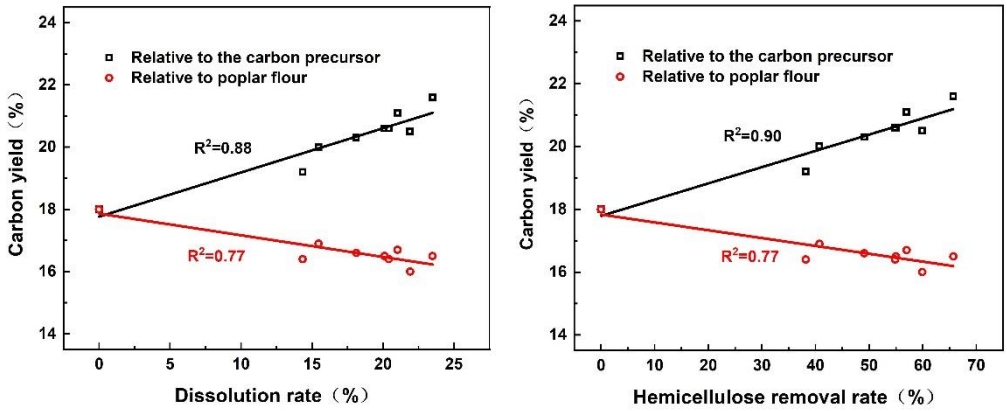

Fig. 5. The relationship between dissolution rate / hemicellulose removal rate and activated carbon yield

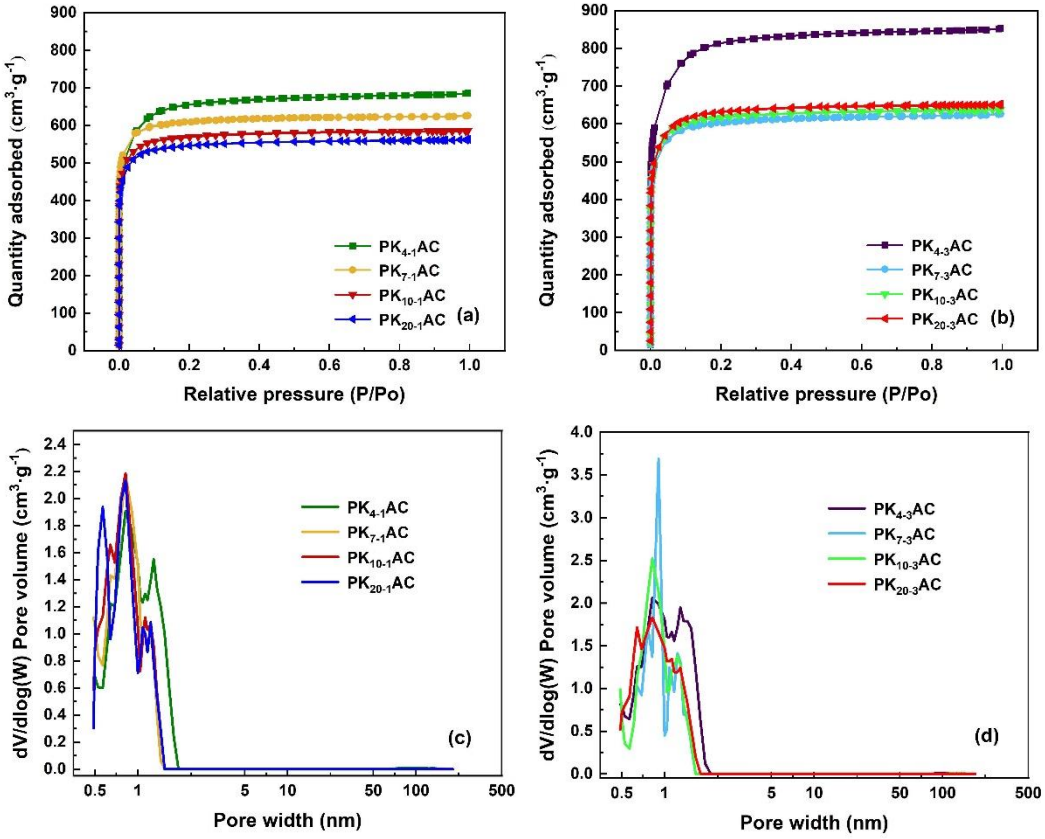

Fig. 6. N_2 adsorption/desorption isotherms (a, b) and pore size distributions (c, d) of activated carbons prepared with $PK_{x\text{-}y}$ as carbon precursors

Table 4. Yield and Main Pore Structure Parameters of Activated Carbons Prepared with PK_{x-Y} as Carbon Precursors

Sample	[1]Carbon yield (%)	[2]S_{BET} ($m^2 \cdot g^{-1}$)	[3]S_{micro} ($m^2 \cdot g^{-1}$)	[4]S_{meso} ($m^2 \cdot g^{-1}$)	[5]S_{ultra} ($m^2 \cdot g^{-1}$)	[6]V_{total} ($cm^3 \cdot g^{-1}$)	[3]V_{micro} ($cm^3 \cdot g^{-1}$)	[4]V_{meso} ($cm^3 \cdot g^{-1}$)	[5]V_{ultra} ($cm^3 \cdot g^{-1}$)	[7]D_p (nm)
PAC	18.0	1401	1337	61	582	0.59	0.51	0.08	0.22	1.67
$PK_{4-1}AC$	16.4	2500	2039	237	338	1.06	0.81	0.15	0.13	1.70
$PK_{7-1}AC$	16.6	2434	2234	127	604	0.97	0.85	0.08	0.24	1.59
$PK_{10-1}AC$	16.5	2239	2109	95	483	0.91	0.82	0.06	0.14	1.62
$PK_{20-1}AC$	16.0	2154	2032	93	633	0.87	0.79	0.06	0.18	1.61
$PK_{4-3}AC$	16.9	3066	2374	327	302	1.32	0.95	0.22	0.13	1.72
$PK_{7-3}AC$	16.4	2401	2245	121	611	0.99	0.89	0.08	0.21	1.64
$PK_{10-3}AC$	16.7	2500	2221	162	363	1.02	0.87	0.10	0.18	1.64
$PK_{20-3}AC$	16.5	2458	2298	129	390	1.01	0.91	0.08	0.12	1.64
Note: [1]Carbon yield, [2]S_{BET}, [3]S_{micro}, [3]V_{micro},[4]S_{meso}, [4]V_{meso}, [5]S_{ultra}, [5]V_{ultra}, [6]V_{total}, [7]D_p consistent with Table 2.										

Adsorption Performance of Activated Carbons for VOCs

The VOCs adsorption capacity of activated carbon was affected by both the pore structure of activated carbon and the molecular properties of VOCs. Figure 7a through 7c shows the breakthrough curves of toluene adsorption, and Fig. 7d through 7f shows the breakthrough curves of dichloromethane adsorption. The adsorption capacity of toluene and dichloromethane calculated according to Fig. 7 is listed in Table 5. The results show that the adsorption capacity of toluene on the activated carbons prepared after pretreatment (organic solvent extraction, alkali extraction, or both) is greatly increased. The saturated adsorption capacity of PEAC for toluene was increased from 378 $m^2 \cdot g^{-1}$ to 573 $m^2 \cdot g^{-1}$ (about 51.6% increase), compared with PAC, indicating that the extraction of organic solvent improved the adsorption capacity of toluene. In addition, the adsorption capacity of $P_EK_{20-3}AC$ (521 $m^2 \cdot g^{-1}$) for toluene is only higher than that of PAC (378 $m^2 \cdot g^{-1}$) and lower than that of $PK_{x-y}AC$ (649 through 733$m^2 \cdot g^{-1}$), which is consistent with the change of specific surface area. The saturated adsorption capacity of $PK_{x-y}AC$ for toluene was increased from 378$m^2 \cdot g^{-1}$ to 649 through 733 $m^2 \cdot g^{-1}$ (about 71.7 through 93.9% increase), compared with PAC, indicating that the adsorption capacity of activated carbons for toluene was greatly improved after the selective dissolution of hemicellulose in poplar wood. It is well known that the adsorption capacity of porous carbon materials to VOCs is mainly determined by micropores (Zhang *et al*. 2017)， so the excellent adsorption capacity of $PK_{x-y}AC$ to toluene is mainly caused by its developed microporous structure. This view has also been proved in some studies. It has been reported that micropores provide the main adsorption sites, while mesopores enhance intra-particle diffusion and shorten the adsorption time. Therefore, different pore sizes have different effects on the VOCs adsorption of carbon materials. It is even reported that micropores, especially narrow micropores, play a leading role in the VOCs adsorption of carbon materials. However, the increase of diffusion resistance in narrow pores may lead to a low adsorption rate.

Surprisingly, Fig. 7d through 7f and Table 5 show that the adsorption performance of poplar-based activated carbons for dichloromethane is different from that of toluene or even the opposite. Among all samples, $PK_{4-3}AC$ has the highest specific surface area, pore volume, and toluene adsorption capacity, but its saturated adsorption capacity for

dichloromethane (105 mg·g^{-1}) is the lowest; PAC has the lowest specific surface area, pore volume, and toluene adsorption capacity, but its saturated adsorption capacity for dichloromethane (184 mg·g^{-1}) is the highest, and the adsorption capacity of all activated carbons for toluene is noticeably higher than that of dichloromethane. To study the relationship between the adsorption capacity of toluene/dichloromethane and the pore structures of activated carbons, this study tried to explain this phenomenon from the perspective of the pore distribution of activated carbon and molecular dynamics diameter of VOCs. It is well known that the molecular dynamic diameters of toluene and dichloromethane are 0.67 nm and 0.33 nm, respectively. The relationship between pore structure parameters (S_{BET}, S_{micro}, S_{ultra}) and adsorption capacity of toluene / dichloromethane was plotted in Fig. 8 by linear fitting. The results show that the adsorption capacity of toluene has a good correlation with Smicro and Vmicro (R^2 = 0.9547, R^2 = 0.9595), and the adsorption capacity of dichloromethane is more closely related to Sultra and Vultra (R^2 = 0.4804, R^2 = 0.5026), which indicates that the adsorption of toluene is mainly determined by micropores, and the adsorption of dichloromethane is more closely related to micropores in these samples. It should be pointed out here that because these samples are activated carbon with a high proportion of micropores, the adsorption amount of toluene is also closely related to the total specific surface area and total pore volume. However, it is undeniable that there are still many other factors affecting adsorption in the actual adsorption process (Zhu *et al*. 2018). It can be concluded that the reason why PAC has a higher adsorption capacity of dichloromethane is that it has a superior ultramicroporous structure. Moreover, the adsorption capacity of activated carbons for dichloromethane is less than that of toluene because the volume of the ultramicropore is less than that of the micropore. This is consistent with previous studies, that is, when the main pore diameter of the porous adsorbent is 1 to 3 times the molecular dynamics diameter of the target VOCs, the adsorption capacity increases noticeably (Lozano-Castello *et al*. 2002; Zhang *et al*. 2019a). In this study, the selective extraction of hemicellulose has brought a more developed microporous structure to activated carbons, and the pores changed from ultramicropores (less than 0.6 nm) to larger micropores (0.6 through 2 nm). In addition, different pore distribution leads to the different adsorption capacity of activated carbons for VOCs with different molecular diameters. The best adsorption occurs at the place where the pore size matches the size of the adsorbate. Therefore, ultra-micropores are more suitable for the adsorption of dichloromethane with smaller molecular diameters.

It is undeniable that the poplar-based activated carbons prepared in this study has a long penetration time and satisfactory adsorption capacity for toluene and dichloromethane. Among them, the adsorption capacity of $PK_{4\text{-}3}AC$ for toluene is up to 733 mg·g^{-1}, higher than that of commercial activated carbons and other carbon materials based on the traditional carbonization /activation process, and the adsorption capacity of PAC for dichloromethane is up to 184 mg·g^{-1}. Table 6 shows the adsorption capacity of other carbon materials for toluene and dichloromethane, and compares it with the activated carbons obtained in this study.

The Yoon-Nelson model is used to fit the adsorption data, and the fitting parameters are shown in Table 7. The results show that the Yoon-Nelson model has a good fitting effect on the toluene/dichloromethane breakthrough curves of poplar-based activated carbons, indicating that the Yoon-Nelson model can well predict the VOCs adsorption of activated carbons. In contrast, the KYN of dichloromethane is noticeably higher than that of toluene, indicating that the mass transfer resistance of dichloromethane in the activated

carbons is lower and it can penetrate the adsorbents faster, which is related to the smaller molecular dynamics diameter of dichloromethane.

In conclusion, the adsorption capacities of toluene and dichloromethane are closely related to micropores (< 2 nm) and ultramicropores (< 0.6 nm) of activated carbons, respectively. $PK_{x\text{-}y}AC$ is a toluene adsorbent with excellent performance because of its high proportion of microporous structure, and PAC has more advantages in the adsorption of dichloromethane because of its more abundant ultramicropores. Furthermore, the pre-extraction of hemicellulose greatly improves the VOCs adsorption capacity of activated carbons by increasing the micropores.

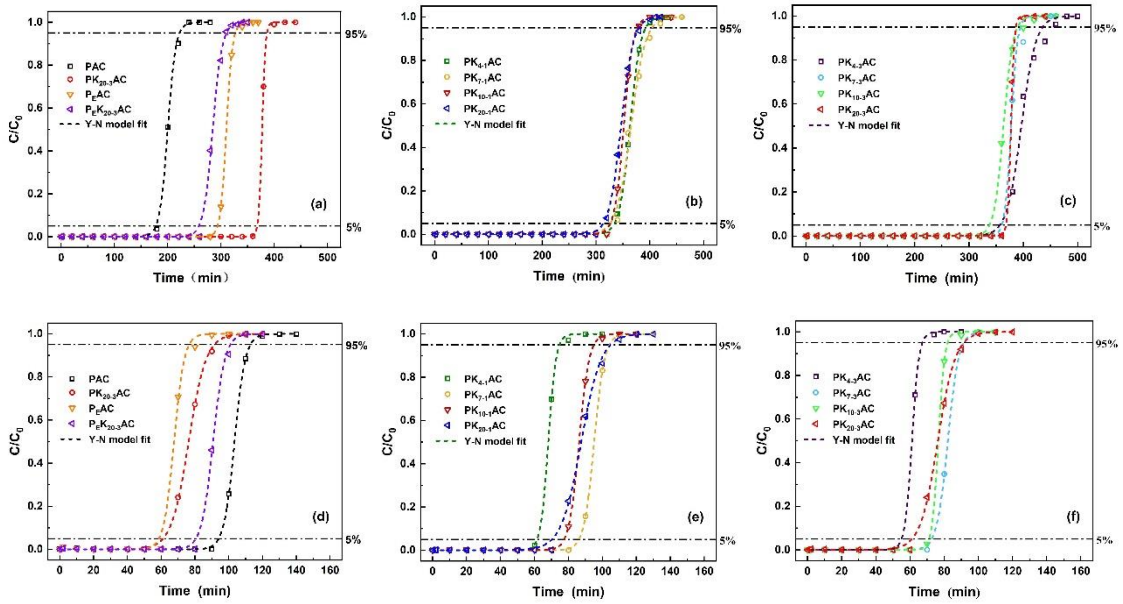

Fig. 7. Breakthrough curves of activated carbons for toluene (a through c) / dichloromethane (d through f)

Table 5. Adsorption Capacity of VOCs on Activated Carbons

Sample	Adsorption Capacity ($mg \cdot g^{-1}$)			
	Toluene		Dichloromethane	
	Qb	Qs	Qb	Qs
PAC	337	378	164	184
P_EAC	530	573	107	118
$PK_{4\text{-}1}AC$	612	673	106	118
$PK_{7\text{-}1}AC$	631	676	144	165
$PK_{10\text{-}1}AC$	621	667	131	151
$PK_{20\text{-}1}AC$	589	649	127	154
$PK_{4\text{-}3}AC$	671	733	90	105
$PK_{7\text{-}3}AC$	667	702	124	143
$PK_{10\text{-}3}AC$	635	674	123	133
$PK_{20\text{-}3}AC$	683	711	110	135
$P_EK_{20\text{-}3}AC$	477	521	140	157

Table 6. Adsorption Capacity of VOCs on Different Carbon Materials

Sample	S_{BET} ($m^2 \cdot g^{-1}$)	Condition	VOCs Adsorption Capacity ($mg \cdot g^{-1}$)	Citations
$PK_{4\text{-}3}AC$	3066	30 °C, 100 $mL \cdot min^{-1}$, 500 ppm	733 (Toluene)	This work
PAC	1401	30 °C, 100 $mL \cdot min^{-1}$, 500 ppm	184 (Dichloromethane)	This work
Commercial activated carbon	885	30 °C, 100 $mL \cdot min^{-1}$, 500 ppm	295 (Toluene) 87 (Dichloromethane)	Taken from the laboratory medicine cabinet
Corncob-based activated carbon (CBAC-1.0-1.0-550)	1501	25 °C, 500 $mL \cdot min^{-1}$, 3000 $mg \cdot m^{-3}$	416.6 (Toluene)	Zhu *et al.* (2018)
Pine bark activated carbon (H_3PO_4-AC)	3342	20 °C, 70 $mL \cdot min^{-1}$, 2.5%VOC/N_2 (2.5×10^4 ppm)	506 (Toluene)	Sessa *et al.* (2022)
Defatted black cumin activated carbon (DBCB-AC)	1213	25 °C, 100 $mL \cdot min^{-1}$, 20 mg/L	580 (Toluene)	Batur and Kutluay (2022)
Activated carbon after nitric acid treatment (AC-MkN)	856	35 °C , 100 $mL \cdot min^{-1}$, 995 ppm	123.9 (Dichloromethane)	Lemus *et al.* (2012)
Activated carbon modified by metal ions (Al(III)/AC)	828	25 °C, 0.667 $mL \cdot s^{-1}$, 8.825 $g \cdot m^{-3}$	43 (Dichloromethane)	Pan *et al.* (2013)
Activated carbon from *Digitalis purpurea* L. biomass (D_pAC58)	1753.5	25 °C, 50 $mL \cdot min^{-1}$, 1500 ppm	162 (Benzene, toluene, ethylbenzene, and xylene, known as BTEX)	Isinkaralar (2022b)
Activated carbon from *Althaea officinalis* L. biomass (Ao-AC43)	1424	25 °C, 50 $mL \cdot min^{-1}$, 1500 ppm	140 (Benzene)	Isinkaralar (2022a)

Table 7. Y-N Model Fitting Parameters of Activated Carbons

Sample	Y-N Model Fitting Parameters					
	Toluene			Dichloromethane		
	K_{YN} (min^{-1})	τ (min)	R^2	K_{YN} (min^{-1})	τ (min)	R^2
PAC	0.1317	200	0.9991	0.3122	103	0.9998
P_EAC	0.1760	310	0.9999	0.3291	68	0.9969
$PK_{4\text{-}1}AC$	0.1017	363	0.9999	0.4409	68	0.9997
$PK_{7\text{-}1}AC$	0.0757	365	0.9967	0.3276	95	0.9999
$PK_{10\text{-}1}AC$	0.1171	352	0.9998	0.3356	86	0.9999
$PK_{20\text{-}1}AC$	0.0883	347	0.9998	0.1703	88	0.9986
$PK_{4\text{-}3}AC$	0.0747	396	0.9948	0.4787	61	0.9999
$PK_{7\text{-}3}AC$	0.1720	378	0.9968	0.3124	82	0.9997
$PK_{10\text{-}3}AC$	0.1143	364	0.9983	0.5417	77	0.9999
$PK_{20\text{-}3}AC$	0.3174	377	0.9999	0.1938	76	0.9992
$P_EK_{20\text{-}3}AC$	0.1138	285	0.9986	0.2881	91	0.9986

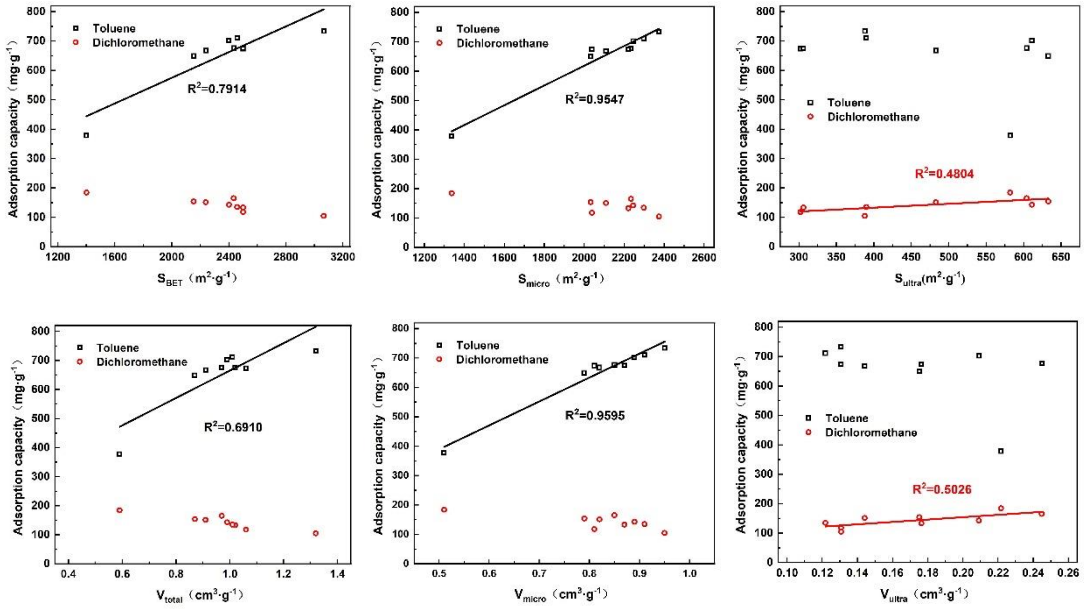

Fig. 8. The relationship between pore structure parameters and adsorption capacity of toluene / dichloromethane

CONCLUSIONS

1. The pre-extraction of hemicellulose could noticeably increase the microporous surface area and microporous pore volume of poplar-based activated carbons, thus greatly enhancing the adsorption capacity of VOCs.
2. The removal rate of hemicellulose and the yields of activated carbons under alkali extraction were less affected by the pre-extraction of organic solvent.
3. After the selective pre-extraction of 38.18 to 65.70 wt% hemicellulose from poplar, the final yield of activated carbons only decreased 1.1 to 2.0%, but the pore structure of activated carbons was greatly improved. A total of 40.74 wt% hemicellulose in poplar was removed under 4 wt% alkali concentration and 3 h KOH treatment, the activated

carbon prepared from HPR gave the highest BET surface area and pore volume; 3066 $m^2 \cdot g^{-1}$ and 1.32 $cm^3 \cdot g^{-1}$, respectively. The pore structures of activated carbons can be controlled to some extent by changing the removal degree of hemicellulose.

4. The adsorption results of VOCs show that because of the rich microporous and ultramicroporous structures, the adsorption capacity of $PK_{4\text{-}3}AC$ for toluene is 733 $mg \cdot g^{-1}$, and that of PAC for dichloromethane is 184 $mg \cdot g^{-1}$, which are better than the previously reported adsorbents. Furthermore, the adsorption capacities of toluene and dichloromethane are closely related to micropores (< 2 nm) and ultramicropores (< 0.6 nm) of activated carbons, respectively.

ACKNOWLEDGMENTS

The authors greatly acknowledge the support of the Natural Sciences Foundation of China (No. 32271807).

REFERENCES CITED

Arzami, A. N., Ho, T. M., and Mikkonen, K. S. (2022). "Valorization of cereal by-product hemicelluloses: Fractionation and purity considerations," *Food Research International* 151, Article ID 110818. DOI: 10.1016/j.foodres.2021.110818

Basta, A. H., Fierro, V., Ei-Saied, H., and Celzard, A. (2009). "2-Steps KOH activation of rice straw: An efficient method for preparing high-performance activated carbons," *Bioresource Technology* 100(17), 3941-3947. DOI: 10.1016/j.biortech.2009.02.028

Batur, E., and Kutluay, S. (2022). "Dynamic adsorption behavior of benzene, toluene, and xylene VOCs in single- and multi-component systems by activated carbon derived from defatted black cumin (*Nigella sativa* L.) biowaste," *Journal of Environmental Chemical Engineering* 10(3), Article ID 107565. DOI: 10.1016/j.jece.2022.107565

Benoît, C., Xavier, P., André, G., Fritz, S., and Gérard, C. (2008). "Contributions of hemicellulose, cellulose and lignin to the mass and the porous properties of chars and steam activated carbons from various lignocellulosic precursors," *Bioresource Technology* 100(1), 292-298. DOI: 10.1016/j.biortech.2008.06.009

Chen, Y. W., and Lee, H. V. (2020). "Recent progress in homogeneous Lewis acid catalysts for the transformation of hemicellulose and cellulose into valuable chemicals, fuels, and nanocellulose," *Reviews in Chemical Engineering* 36(2), 215-235. DOI: 10.1515/revce-2017-0071

Collard, F. X., and Blin, J. (2014). "A review on pyrolysis of biomass constituents: Mechanisms and composition of the products obtained from the conversion of cellulose, hemicelluloses and lignin," *Renewable and Sustainable Energy Reviews* 38, 594-608. DOI: 10.1016/j.rser.2014.06.013

David, E., and Niculescu, V. C. (2021). "Volatile organic compounds (VOCs) as environmental pollutants: Occurrence and mitigation using nanomaterials," *International Journal of Environmental Research and Public Health* 18(24), Article ID 13147. DOI: 10.3390/ijerph182413147

Deng, S. B., Nie, Y., Du, Z. W., Huang, Q., Meng, P. P., Wang, B., Huang, J., and Yu, G. (2015). "Enhanced adsorption of perfluorooctane sulfonate and perfluorooctanoate by bamboo-derived granular activated carbon," *Journal of Hazardous Materials* 282, 150-157. DOI: 10.1016/j.jhazmat.2014.03.045

Enesca, A., and Cazan, C. (2020). "Volatile organic compounds (VOCs) removal from indoor air by heterostructures/composites/doped photocatalysts: A mini-review," *Nanomaterials* 10(10), Article Number 1965. DOI: 10.3390/nano10101965

Garcia, J. C., Alfaro, A., Loaiza, J. M., Lozano-Calvo, S., and Lopez, F. (2022). "Cold alkaline extraction of elephant grass for optimal subsequent extraction of hemicelluloses and energy production," *Biomass Conversion and Biorefinery* (Online). DOI: 10.1007/s13399-022-03054-3

GB/T 744 (2004). "Pulps-Determination of alkali resistance," Standardization Administration of China, Beijing, China.

GB/T 35818 (2018). "Standard method for analysis of forestry biomass-Determination of structural polysaccharides and lignin," Standardization Administration of China, Beijing, China.

Gil, R. R., Ruiz, B., Lozano, M. S., Martin, M. J., and Fuente, E. (2014). "VOCs removal by adsorption onto activated carbons from biocollagenic wastes of vegetable tanning," *Chemical Engineering Journal* 245, 80-88. DOI: 10.1016/j.cej.2014.02.012

Guo, Y. F., Tan, C., Sun, J., Li, W. L., Zhang, J. B., and Zhao, C. W. (2020). "Porous activated carbons derived from waste sugarcane bagasse for CO2 adsorption," *Chemical Engineering Journal* 381, Article ID 122736. DOI: 10.1016/j.cej.2019.122736

Isinkaralar, K. (2022a). "High-efficiency removal of benzene vapor using activated carbon from *Althaea officinalis* L. biomass as a lignocellulosic precursor," *Environmental Science and Pollution Research* 29, 66728–66740. DOI: 10.1007/s11356-022-20579-2

Isinkaralar, K. (2022b). "Theoretical removal study of gas BTEX onto activated carbon produced from *Digitalis purpurea* L. biomass," *Biomass Conversion and Biorefinery* 12(9), 4171-4181. DOI: 10.1007/s13399-022-02558-2

Lemus, J., Martin-Martinez, M., Palomar, J., Gomez-Sainero, L., Gilarranz, M. A., and Rodriguez, J. J. (2012). "Removal of chlorinated organic volatile compounds by gas phase adsorption with activated carbon," *Chemical Engineering Journal* 211, 246-254. DOI: 10.1016/j.cej.2012.09.021

Li, X. Q., Zhang, L., Yang, Z. Q., He, Z. Q., Wang, P., Yan, Y. F., and Ran, J. Y. (2020). "Hydrophobic modified activated carbon using PDMS for the adsorption of VOCs in humid condition," *Separation and Purification Technology* 239, Article ID 116517 DOI: 10.1016/j.seppur.2020.116517

Li, Z., Li, Y. H., and Zhu, J. (2021). "Straw-based activated carbon: optimization of the preparation procedure and performance of volatile organic compounds adsorption," *Materials* 14(12), Article ID 3284. DOI: 10.3390/ma14123284

Liu, X., Wan, Y. B., Liu, P. L., Fu, Y. Z., and Zou, W. H. (2018). "A novel activated carbon prepared from grapefruit peel and its application in removal of phenolic compounds," *Water Science and Technology* 77(10), 2517-2527. DOI: 10.2166/wst.2018.212

Lozano-Castello, D., Cazorla-Amoros, D., Linares-Solano, A., and Quinn, D. F. (2002). "Influence of pore size distribution on methane storage at relatively low pressure:

preparation of activated carbon with optimum pore size," *Carbon* 40(7), 989-1002. DOI: 10.1016/S0008-6223(01)00235-4

Magoling, B., and Macalalad, A. A. (2017). "Optimization and response surface modelling of activated carbon production from mahogany fruit husk for removal of chromium (VI) from aqueous solution," *BioResources* 12(2), 3001-3016. DOI: 10.15376/biores.12.2.3001-3016

Pan, H. Y., Tian, M., Zhang, H., Zhang, Y., and Lin, Q. (2013). "Adsorption and desorption performance of dichloromethane over activated carbons modified by metal ions," *Journal Of chemical and Engineering Data* 58(9), 2449-2454. DOI: 10.1021/je4003493

Peng, F., Bian, J., Ren, J. L., Peng, P., Xu, F., and Sun, R. C. (2012). "Fractionation and characterization of alkali-extracted hemicelluloses from pea shrub," *Biomass and Bioenergy* 39, 20-30. DOI: 10.1016/j.biombioe.2010.08.034

Pui, W. K., Yusoff, R., and Aroua, M. K. (2019). "A review on activated carbon adsorption for volatile organic compounds (VOCs)," *Reviews in Chemical Engineering* 35(5), 649-668. DOI: 10.1515/revce-2017-0057

Scapini, T., Dos Santos, M., Bonatto, C., Wancura, J., Mulinari, J., Camargo, A. F., Klanovicz, N., Zabot, G. L., Tres, M. V., Fongaro, G., *et al*. (2021). "Hydrothermal pretreatment of lignocellulosic biomass for hemicellulose recovery," *Bioresource Technology* 342, Article ID 126033. DOI: 10.1016/j.biortech.2021.126033

Sessa, F., Merlin, G., and Canu, P. (2022). "Pine bark valorization by activated carbons production to be used as VOCs adsorbents," *Fuel* 318, Article ID 123346. DOI: 10.1016/j.fuel.2022.123346

Sun, D., Lv, Z. W., Rao, J., Tian, R., Sun, S. N., and Peng, F. (2022). "Effects of hydrothermal pretreatment on the dissolution and structural evolution of hemicelluloses and lignin: A review," *Carbohydrate Polymers* 281, Article ID 119050. DOI: 10.1016/j.carbpol.2021.119050

Wang, H. H., Wang, X., Cui, Y. S., Xue, Z. C., and Ba, Y. X. (2018). "Slow pyrolysis polygeneration of bamboo (*Phyllostachys pubescens*): Product yield prediction and biochar formation mechanism," *Bioresource Technology* 263, 444-449. DOI: 10.1016/j.biortech.2018.05.040

Wang, C., Zou, R., Qian, M., Kong, X., Huo, E., Lin, X., Wang, L., Zhang, X., Ruan, R., and Lei, H. (2022). "Improvement of the carbon yield from biomass carbonization through sulfuric acid pre-dehydration at room temperature," *Bioresource Technology* 355, Article ID 127251. DOI: 10.1016/j.biortech.2022.127251

Xu, J. S., Xiao, Y. A., Zhang, J. F., Shang, Z., Tian, Z. S., Zhu, X. L., Li, K., and Liu, Y. X. (2022). "Microwave expansion pretreatment for enhancing microwave-assisted alkaline extraction of hemicellulose from bagasse," *Biomass Conversion and Biorefinery* (Online). DOI: 10.1007/s13399-022-03220-7

Yagmur, E., Tunc, M. S., Banford, A., and Aktas, Z. (2013). "Preparation of activated carbon from autohydrolysed mixed southern hardwood," *Journal of Analytical and Applied Pyrolysis* 104, 470-478. DOI: 10.1016/j.jaap.2013.05.025

Yan, F., Tian, S. Q., Du, K., and Wang, X. W. (2021). "Effects of steam explosion pretreatment on the extraction of xylooligosaccharide from rice husk," *BioResources* 16(4), 6909-6919. DOI: 10.15376/biores.16.4.6910-6920

Yang, F., Lu, Y. T., Li, W. H., Tu, W. L., Li, L. L., Wang, X. Y., Yuan, A., and Pan, J. M. (2021). "Route-optimized synthesis of bagasse-derived hierarchical activated carbon for maximizing volatile organic compound (VOC) adsorption capture properties," *ChemistrySelect* 6(38), 10362-10368. DOI: 10.1002/slct.202101295

Yang, F., Li, W. H., Zhong, X., Tu, W. L., Cheng, J., Chen, L., Lu, J., Yuan, A., and Pan, J. M. (2022a). "The alkaline sites integrated into biomass-carbon reinforce selective adsorption of acetic acid: In situ implanting MgO during activation operation," *Separation and Purification Technology* 297,121415. DOI: 10.1016/j.seppur.2022.121415

Yang, J. Y., Zhang, W. J., Wang, Y., Li, M. F., Peng, F., and Bian, J. (2022b). "Novel, recyclable Bronsted acidic deep eutectic solvent for mild fractionation of hemicelluloses," *Carbohydrate Polymers* 278, Article ID 118992. DOI: 10.1016/j.carbpol.2021.118992

Yoon, Y. H., and Nelson, J. H. (1984). "Application of gas adsorption kinetics--II. A theoretical model for respirator cartridge service life and its practical applications," *American Industrial Hygiene Association Journal* 45(8), 517-524.

Yuan, Z. Y., Kapu, N. S., Beatson, R., Chang, X. F., and Martinez, D. M. (2016). "Effect of alkaline pre-extraction of hemicelluloses and silica on kraft pulping of bamboo (*Neosinocalamus affinis* Keng)," *Industrial Crops and Products* 91, 66-75. DOI: 10.1016/j.indcrop.2016.06.019

Zhang, X. Y., Gao, B., Creamer, A. E., Cao, C. C., and Li, Y. C. (2017). "Adsorption of VOCs onto engineered carbon materials: A review," *Journal of Hazardous Materials* 338, 102-123. DOI: 10.1016/j.jhazmat.2017.05.013

Zhang, W. X., Cheng, H. R., Niu, Q., Fu, M. L., Huang, H. M., and Ye, D. Q. (2019a). "Microbial targeted degradation pretreatment: A novel approach to preparation of activated carbon with specific hierarchical porous structures, high surface areas, and satisfactory toluene adsorption performance," *Environmental Science and Technology* 53(13), 7632-7640. DOI: 10.1021/acs.est.9b01159

Zhang, Z. K., Zhu, Z. Y., Shen, B. X., and Liu, L. N. (2019b). "Insights into biochar and hydrochar production and applications: A review," *Energy* 171, 581-598. DOI: 10.1016/j.energy.2019.01.035

Zhang, Z. B., Jiang, C., Li, D. W., Lei, Y. Q., Yao, H. M., Zhou, G. Y., Wang, K., Rao, Y. L., Liu, W. G., Xu, C. L., *et al.* (2020). "Micro-mesoporous activated carbon simultaneously possessing large surface area and ultra-high pore volume for efficiently adsorbing various VOCs," *Carbon* 170, 567-579. DOI: 10.1016/j.carbon.2020.08.033

Zhao, Y. L., Sun, H., Yang, B., and Weng, Y. X. (2020). "Hemicellulose-based film: Potential green films for food packaging," *Polymers* 12(8), Article ID 1775. DOI: 10.3390/polym12081775

Zhou, K., Ma, W. W., Zeng, Z., Ma, X. C., Xu, X., Guo, Y., Li, H. L., and Li, L. Q. (2019). "Experimental and DFT study on the adsorption of VOCs on activated carbon/metal oxides composites," *Chemical Engineering Journal* 372, 1122-1133. DOI: 10.1016/j.cej.2019.04.218

Zhu, J., Li, Y. H., Xu, L., and Liu, Z. Y. (2018). "Removal of toluene from waste gas by adsorption-desorption process using corncob-based activated carbons as adsorbents," *Ecotoxicology and Environmental Safety* 165, 115-125. DOI: 10.1016/j.ecoenv.2018.08.105

Article submitted: December 6, 2022; Peer review completed: January 21, 2023; Revised version received; February 13, 2023; Accepted: February 16, 2023; Published: February 27, 2023.
DOI: 10.15376/biores.18.2.2874-2896